metals

MDPI

Article

Statistical Analysis-Based Prediction Model for Fatigue Characteristics in Lap Joints Considering Weld Geometry, Including Gaps

Dong-Yoon Kim and Jiyoung Yu *

Flexible Manufacturing R&D Department, Korea Institute of Industrial Technology, Incheon 21999, Republic of Korea; kimdy@kitech.re.kr
* Correspondence: willow@kitech.re.kr

Abstract: Automotive chassis components, constructed as lap joints and produced by gas metal arc welding (GMAW), require fatigue durability. The fatigue properties of the weld in a lap joint are largely determined by weld geometry factors. When there is no gap or a consistent gap in the lap joint, improving the geometry of the weld toe can alleviate stress concentration and enhance fatigue properties. However, due to machining tolerances, it is difficult to completely eliminate or consistently manage the gap in the joint. In the case of a lap-welded joint with an inconsistent gap, it is necessary to identify the weld geometry factors related to fatigue properties. Evaluating the fatigue behavior of materials and welded joints requires significant time and cost, meaning that research that seeks to predict fatigue properties is essential. More research is needed on predicting fatigue properties related to automotive chassis components, particularly studies on predicting the fatigue properties of lap-welded joints with gaps. This study proposed a regression model for predicting fatigue properties based on crucial weld geometry factors in lap-welded joints with gaps using statistical analysis. Welding conditions were varied in order to build various weld geometries in joints configured in a lap with gaps of 0, 0.2, 0.5, and 1.0 mm, and 87 S–N curves for the lap-welded joints were derived. As input variables, 17 weld geometry factors (7 lengths, 7 angles, and 3 area factors) were selected. The slope of the S–N curve using the Basquin model from the S–N curve and the safe fatigue strength were selected as output variables for prediction in order to develop the regression model. Multiple linear regression models, multiple non-linear regression models, and second-order polynomial regression models were proposed to predict fatigue properties. Backward elimination was applied to simplify the models and reduce overfitting. Among the three proposed regression models, the multiple non-linear regression model had a coefficient of determination greater than 0.86. In lap-welded joints with gaps, the weld geometry factors representing fatigue properties were identified through standardized regression coefficients, and four weld geometry factors related to stress concentration were proposed.

Keywords: lap-welded joint; GMAW; fatigue characteristic prediction; regression model; joint gap; weld geometry

Citation: Kim, D.-Y.; Yu, J. Statistical Analysis-Based Prediction Model for Fatigue Characteristics in Lap Joints Considering Weld Geometry, Including Gaps. *Metals* **2024**, *14*, 1106. https://doi.org/10.3390/met14101106

Academic Editors: Frank Czerwinski and Dariusz Rozumek

Received: 6 August 2024
Revised: 6 September 2024
Accepted: 24 September 2024
Published: 26 September 2024

1. Introduction

The automobile chassis collectively refers to all the parts of a car, excluding the body, and consists of the frame, powertrain, suspension, steering, and braking components. Among these, the frame serves as the fundamental skeleton of the chassis, comprising cross-members, lower arms, and coupled torsion beam axle, and is located at the very bottom of the car, requiring durability against repetitive loads during operation.

The chassis frame, which requires fatigue durability, mainly comprises lap joints and is primarily manufactured using GMAW to ensure strength. In GMAW, using filler wire, the weld metal will inevitably impart a geometric shape to the joint. This acts as

a stress concentration point due to repeated fatigue, leading to fracture initiation and ultimately decreasing the component's fatigue durability. Even when high-strength steel is applied to chassis components for weight reduction, the benefits of high-strength steel are lost due to the notch effect of lap welds [1,2]. In welded joints with geometric shapes, such as lap welds, the bead shape has a more significant impact on fatigue characteristics than does the weld's microstructure [3,4]. Ahiale et al. [4] compared the weld geometry and fatigue characteristics of GMA welds and plasma arc welds in lap joints of 590 MPa-grade dual-phase (DP) steel. Although the heat input in plasma arc welding is relatively higher than that of GMAW, increasing the arc length improves the weld geometry, leading to enhanced fatigue characteristics. Additionally, in the coarse-grain heat-affected zone (CGHAZ), a stress concentration area at the toe, the fraction of acicular ferrite increased in the plasma arc welds. This increase in the acicular ferrite fraction enhances resistance to fatigue crack initiation and early propagation, leading to improved fatigue characteristics. El-Batahgy [5] reproduced the welding thermal cycles of 370 MPa and 500 MPa-grade steels to fabricate CGHAZ specimens and conducted a bending fatigue test. Widmanstatten ferrite exhibited higher tensile strength and fatigue strength compared with polygonal ferrite. Given that the CGHAZ showed higher fatigue strength than the base material, the material's influence on the fatigue strength reduction in lap joint welds is not as significant as the influence of bead geometry. Previous studies have reported that, particularly in lap joints, improving the weld toe angle alleviates stress concentration at the notch area of the weld, thereby enhancing fatigue characteristics [6–10]. Prior investigations examining the fatigue characteristics of lap joints have compared the relationship between weld toe angle and fatigue characteristics only in flawless joints without gaps or in joints with a consistent gap.

Due to deformation during welding and machining dimensional tolerances, the joint gap in welded parts cannot be eliminated or consistently maintained. The presence of gaps in the joint can lead to welding defects, even when welding is performed under the same conditions on identical components [11]. It has been reported that gaps deteriorate fatigue properties [12,13]. Kim et at [14] have reported that, in the welds of lap joints, an increase in the joint gap causes the filler metal of the GMAW process to fill that gap, resulting in a smoother weld profile and an increase in the apparent weld toe angle. However, they confirm that stress concentration at the weld root occurred, leading to decreased fatigue strength. Therefore, they suggest considering geometric shapes other than a weld toe angle for lap welds with gaps requiring fatigue characteristics.

Deriving S–N curves to determine fatigue characteristics is a time-consuming and expensive process. Therefore, methods and research for predicting fatigue characteristics are being actively pursued. After Palmgren introduced the concept of damage accumulation [15] and Miner introduced the linear damage rule [16], many damage and prediction models were developed. Fatemi et al. [17] and Hectors et al. [18] have reviewed an article paper on cumulative damage and life prediction models for fatigue. They have confirmed that linear and non-linear fatigue cumulative damage rules can predict fatigue characteristics based on fatigue life calculations. These calculations reflect the material and weld joint properties and the stress–strain relationship resulting from repetitive loading cycles. Machine learning methods have recently been applied to process data, including noisy data, and learn complex non-linear relationships by which to predict the fatigue characteristics of materials and weldments based on data without prior assumptions. Various machine learning algorithms, including artificial neural networks, convolutional neural networks, residual neural networks, and gradient boosting decision trees, have been applied to predict the fatigue characteristics of materials and weldments, demonstrating excellent fatigue prediction performance [19–22].

In predicting the fatigue characteristics of the lap weld, which is the most commonly used single-sided joint in chassis components, it is considered difficult to apply a fatigue cumulative damage model for load cycles due to the challenge of reflecting the changes to weld shape (non-uniform stress distribution) that arise due to welding conditions and

disturbances during welding. Machine-learning-based prediction models operate as black-box surrogate models between input and output parameters, making the internal decision-making process opaque and difficult to interpret. Additionally, it is challenging to assign physical meaning to the input variables in relation to the output variables [23]. Although studies to fatigue characteristics are being reported for chassis components requiring fatigue properties, research on predicting fatigue characteristics remains relatively scarce. The lack of research on predicting the fatigue characteristics of automotive chassis components is due to the widely accepted fact that improving the weld toe angle of typical lap joints enhances fatigue characteristics. However, the need for additional research on predicting the fatigue characteristics of lap welds, especially considering the gap, is urgent. This is particularly crucial in actual components, where it is impossible to eliminate or maintain a consistent joint gap [11].

This study not only identified the significant weld geometry factors affecting fatigue characteristics in lap welds with gaps but also predicted an S–N curve based on a regression model. Lap welding was performed on GA 590 MPa 2.3 mm, which is widely used in chassis components. The joint gap size (Gap), welding process (WP), wire feed rate (WFR), and welding speed (WS) were varied to achieve different weld geometric shapes. A total of 87 S–N curves were derived through fatigue tests on lap joint specimens with various weld shapes. Through cross-sectional analysis, 17 weld geometry measurements (7 length factors, 7 angle factors, and 3 area factors) were used as input variables. Three regression models were proposed to predict the slope of the S–N curve and the fatigue strength (fatigue strength at 2×10^6 cycles) with a safety factor. Three models were developed using backward elimination: a multiple linear regression model, a multiple non-linear regression model, and a second-order polynomial regression model. The significant factors affecting fatigue characteristics were proposed through standardized regression coefficients.

2. Experimental Procedure

2.1. Welding Procedure

A GA 590 MPa grade steel sheet of thickness 2.3 mm was considered for the welding experiment, and AWS A5.18 ER70S-3 of diameter 1.2 mm was used as the filler wire. Table 1 shows the chemical composition and mechanical properties of the base material and filler wire.

Table 1. The chemical composition and mechanical properties of the base material and filler wire.

	Chemical Composition [wt.%]					**Mechanical Properties**		
	C	**Si**	**Mn**	**P**	**S**	**TS [MPa] ***	**YS [MPa] ***	**EL [%] ***
Base material	0.07	0.14	1.44	0.13	0.002	610	583	25
Filler wire	0.07	0.65	1.14	0.02	0.010	560	440	28

* Note. TS: tensile strength, YS: yield strength, EL: elongation.

The base material was cut to a size of 150 mm × 300 mm, and welding was performed with the specimens overlapped in the rolling direction. As shown in Figure 1, two types of joint orientations were selected. Various weld joint configurations were considered to predict fatigue characteristics through weld joint shapes, and welding was conducted using diverse welding processes and conditions. In order to confirm fatigue characteristics based on joint gap, four gap conditions were selected: 0 mm, 0.2 mm, 0.5 mm, and 1.0 mm. Cold metal transfer (CMT) and direct current (DC) were applied to the two types of joints prepared for the WP. CMT generates a short circuit at a low current and enables welding with low heat input by stably controlling the short circuit through wire feed control [24]. CMT is characterized by a spatter-free metal transfer, excellent gap-bridging ability, and smooth bead formation [25]. The TPS3200CMT (Fronius Co., Petenbach, Austria) welding system was used for CMT, while the DM500 (Daihen Co., Osaka, Japan) welding system was used for DC waveform. The welding system was installed on a robot (GP25, Yaskawa Co.,

Kitakyushu, Japan) to produce the welding specimens through automated welding. The welding parameters were adjusted as follows, and the detailed welding conditions are listed in Table 2. WFR was applied at three levels: 5.0 (setting current/voltage: 165 A/15.2 V), 7.0 (214 A/16.2 V), and 9.0 (258 A/20.5 V) m/min for CMT and 3.0 (140 A/16.8 V), 5.0 (200 A/18.0 V), and 7.0 (254 A/25.7 V) m/min for DC. The welding voltage was applied according to the appropriate voltage conditions provided by the welding power source. Two levels of WS were selected as 60 and 80 cm/min. Additionally, contact tip to work distance (CTWD, α) and work angle were fixed at 15 mm and 45°, respectively. A 90% Ar + 10% CO_2 mixed shielding gas was provided at a flow rate of 25 L/min. The welding experiment was repeated five times under the same conditions to produce a fatigue specimen.

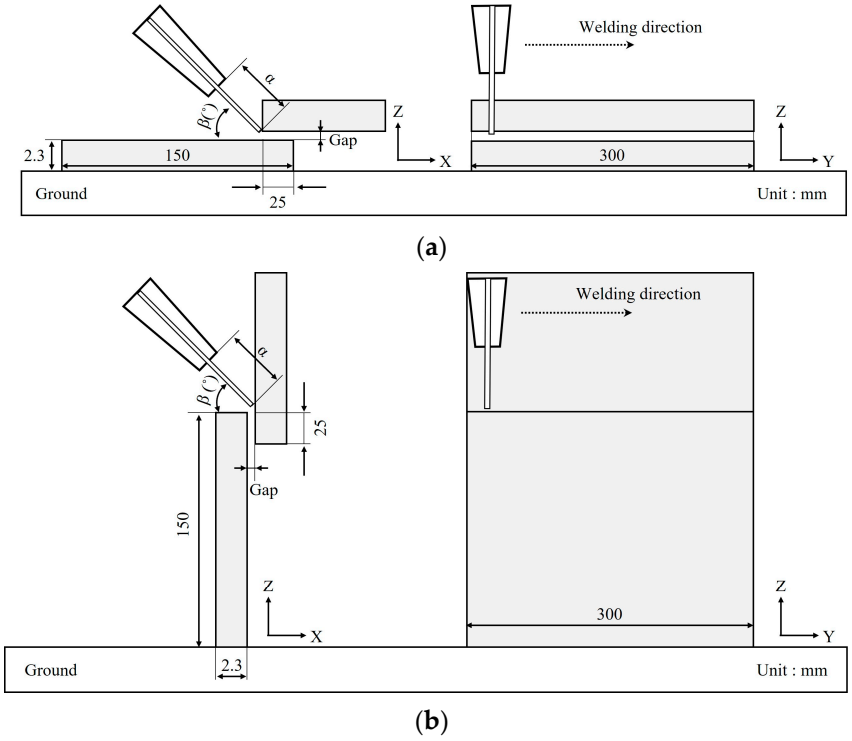

Figure 1. Schematic of joint preparation. (**a**) A position and (**b**) B position.

Table 2. Welding processes and conditions.

Parameters	**Value**			
Weld Joint	**A Position**		**B Position**	
WP	**CMT**	**DC**	**CMT**	**DC**
WFR (m/min) (Setting current/voltage)	5.0 (165 A/15.2 V) 7.0 (214 A/16.2 V) 9.0 (258 A/20.5 V)	3.0 (140 A/16.8 V) 5.0 (200 A/18.0 V) 7.0 (254 A/25.7 V)	5.0 (165 A/15.2 V) 7.0 (214 A/16.2 V) 9.0 (258 A/20.5 V)	3.0 (140 A/16.8 V) 5.0 (200 A/18.0 V) 7.0 (254 A/25.7 V)
WS (cm/min)	60, 80			
Gap (mm)	0, 0.2, 0.5, 1.0			
CTWD (α, mm)	15			
Work angle (β, °)	45			
Shielding gas	90% Ar + 10% CO_2 (25 L/min)			

2.2. Fatigue Test Procedure

The fatigue test specimens were manufactured by referring to the ASTM E466 standard for welding specimens (Figure 2) [26]. A spacer was inserted by combining the thickness

of the gap and base material. During arc welding of GA steel sheet, zinc vaporized by the arc heat can become trapped in the weld metal, leading to porosity defects. These porosity defects together constitute a factor that reduces fatigue life [14]. Figure 3 shows the presence or absence of porosity in the fatigue test specimens as determined by radiographic testing. In this study, we aimed to investigate the relationship between weld geometry factors and fatigue characteristics. To exclude the influence of other factors, such as porosity, we selected fatigue test specimens without porosity defects, as shown in Figure 3a. We employed fatigue testing equipment (Instron 8801, Instron Co., Norwood, MA, USA) with a maximum load of 100 kN. Table 3 show the fatigue test conditions. The stress ratio of a specific component of an automobile chassis was adopted, and the endurance threshold was set at the commonly used 2×10^6 cycles. A total of 87 S–N curves were derived through fatigue testing and were used as data to predict fatigue characteristics. In this study, the fatigue test specimens were denoted in the order of weld joint—WP—WFR—WS—Gap (Table A1). As an example, the following conditions—A position, WP CMT, WFR 7.0 m/min, WS 60 cm/min, Gap 0.2 mm (Table 2)—are expressed as A-C (CMT: C, DC: D)-7.0-60-0.2.

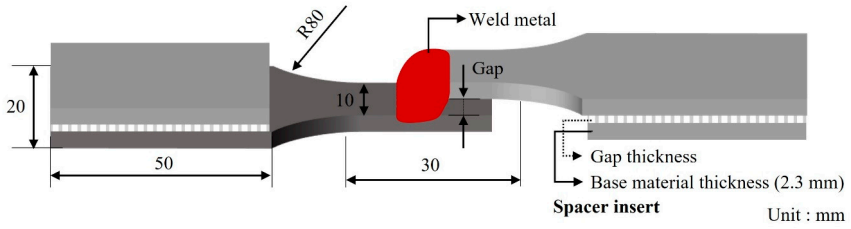

Figure 2. Configuration of fatigue specimen.

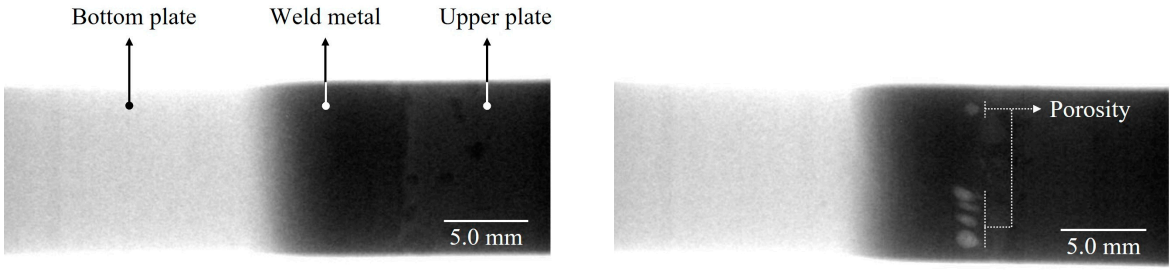

Figure 3. Presence of porosity in fatigue specimens analyzed by radiographic testing (**a**) without porosity and (**b**) with porosity.

Table 3. Fatigue test conditions.

Parameters	Value
Maximum stress (σ_{max})	366–122 MPa (at intervals of 10%)
	122–62 MPa (at intervals of 5%)
	62 MPa under (at intervals of 2.5%)
Stress ratio (R)	0.1
Frequency	40 Hz
Endurance threshold	2×10^6 cycles

3. Method for Developing the S–N Curve Prediction Model

3.1. Selection of Independent and Dependent Variables

Figures A1 and A2 show representative cross-sections after welding with the parameters listed in Table 2. A lap joint weld typically appears in a shape similar to that illustrated

in Figure 4, and the weld joint geometry data were extracted and used as independent variables, as in Figure 4. As criteria for configuration of weld shape to be used in a fatigue prediction model, 17 parameters were extracted. The method for extracting the 17 parameters is summarized in Figure 4. In the geometry of the lap weld joint, seven factors related to length, including leg length and penetration depth [27–30]; seven factors related to angle [31], such as toe angle; and three factors related to area have been derived [31].

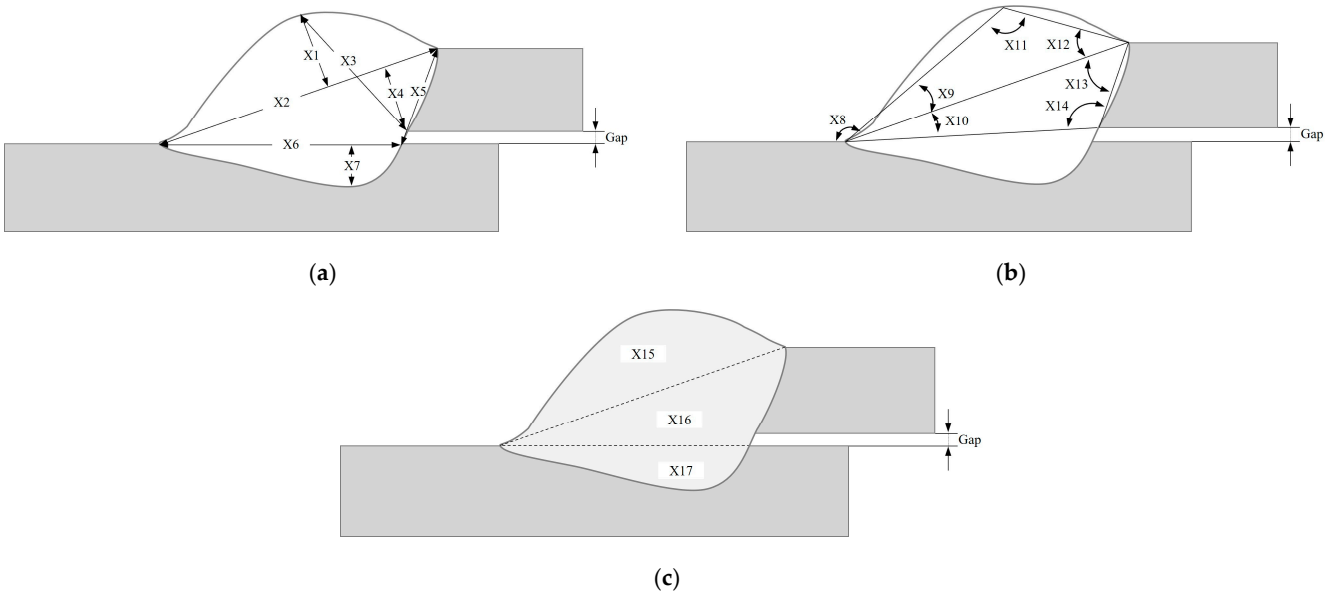

Figure 4. Schematic of weld joint geometry factors for (**a**) length, (**b**) angle, and (**c**) area.

3.2. Selection of Dependent Variables

The response variable for developing the S–N curve prediction model was constructed using the fatigue dataset. For each S–N curve, a logarithm was considered at the stress range (σ_r), and the Basquin equation (Equation (1)) was applied to determine σ'_f and b [32].

$$\sigma = \sigma'_f \cdot \left(N_f\right)^{-b} \tag{1}$$

where σ'_f is the material property, N_f is the fatigue life as the number of cycles to failure under a constant load, and b is the *Basquin slope* (BS).

In the S–N curve for the weld joint, establishing a safety factor to prevent fatigue failure is essential. *Modified* σ'_f (σ'_{f_M}) and *Modified* b (BS_M) were determined by applying M-2SD in Equation (2) [33].

$$N_{M-2SD} = \frac{1}{n}\sum_{i=1}^{n}(N_1 + N_2 + \cdots + N_n) - 2\cdot\sqrt{\frac{1}{n}\sum_{i=1}^{n}\left(N_i - \overline{N}\right)^2} \tag{2}$$

where N represents fatigue life at σ, while $\overline{N}$ signifies the mean life at σ_r.

Essentially, M-2SD represents fatigue life re-expressed by subtracting twice the standard deviation from the average fatigue life at σ_r. This value was used to design a safety factor in the S–N curve using the Basquin equation. BS_M incorporating the safety factor was used as the dependent variable with which to predict fatigue characteristics through weld joint geometry parameters. Only BS_M was predicted, while σ'_{f_M} was not predicted. The reasons are explained in the following section. Predicting the endurance fatigue limit (2×10^6 cycles) on the S–N curve was essential. Fatigue strength at a fatigue life of 2×10^6 cycles was derived from the Basquin equation. using M-2SD and compared with the fatigue strength obtained through fatigue testing. Lower fatigue strength was defined

as safety fatigue strength (SFS), considering stability against fatigue failure. The schematic for σ_{SFS} is presented in Figure 5. The critical factors obtained from BS_M and SFS, along with the individually applied value of stress levels, included independent variables that were used to predict the overall fatigue life. Independent and dependent variables are summarized in Table 4.

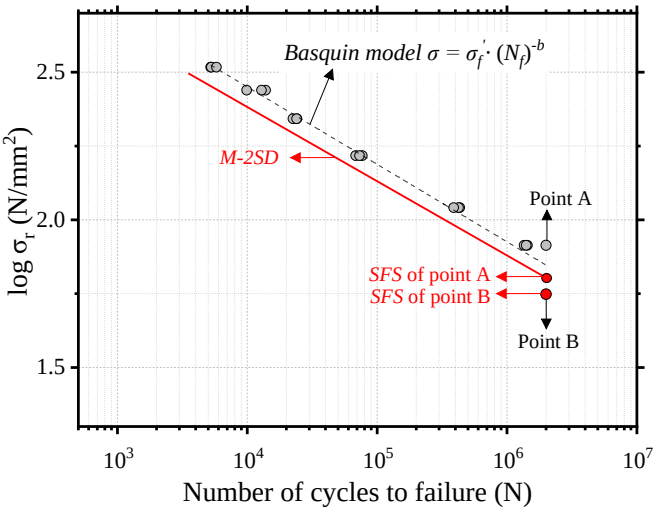

Figure 5. Schematic for the definition of the safety fatigue strength (σ_{SFS}).

Table 4. Independent and dependent variables for predicting fatigue characteristics.

Independent Variable	Dependent Variable.
Seventeen weld geometry factors	BS_M, σ_{SFS}
Significant weld geometry factors	Fatigue life

3.3. Development of an S–N Curve Prediction Model through Statistical Analysis

We employed a statistical analysis method, a regression model approach, to predict the S–N curve. A regression model is a statistical analysis technique used to predict the value of dependent variables from independent variables by assuming a mathematical model between them. A generalized linear regression model was constructed, as given in Equation (3).

$$Y = \beta_0 + \sum_{i=1}^{n} \beta_i f_i(X_0, X_1, \cdots, X_n) + \varepsilon \quad (3)$$

where f_i denotes a scalar function with independent variables as arguments and includes non-linear and polynomial expressions. In this study, multiple linear, non-linear, and second-order polynomial regression models were derived using the backward elimination method.

4. Result of Fatigue Behavior

A total of 87 S–N curves were derived from varying welding conditions, with some of these selectively presented in Figure 6. It was observed that, as WFR increases, fatigue strength and life at a constant load increase (Figure 6a). Conversely, an increase in WS was found to result in decreased fatigue life and strength (Figure 6b). As the gap increased, fatigue life and strength decreased (Figure 6c). The fatigue life and strength were seen to be similar despite changes in the joint position (Figure 6d).

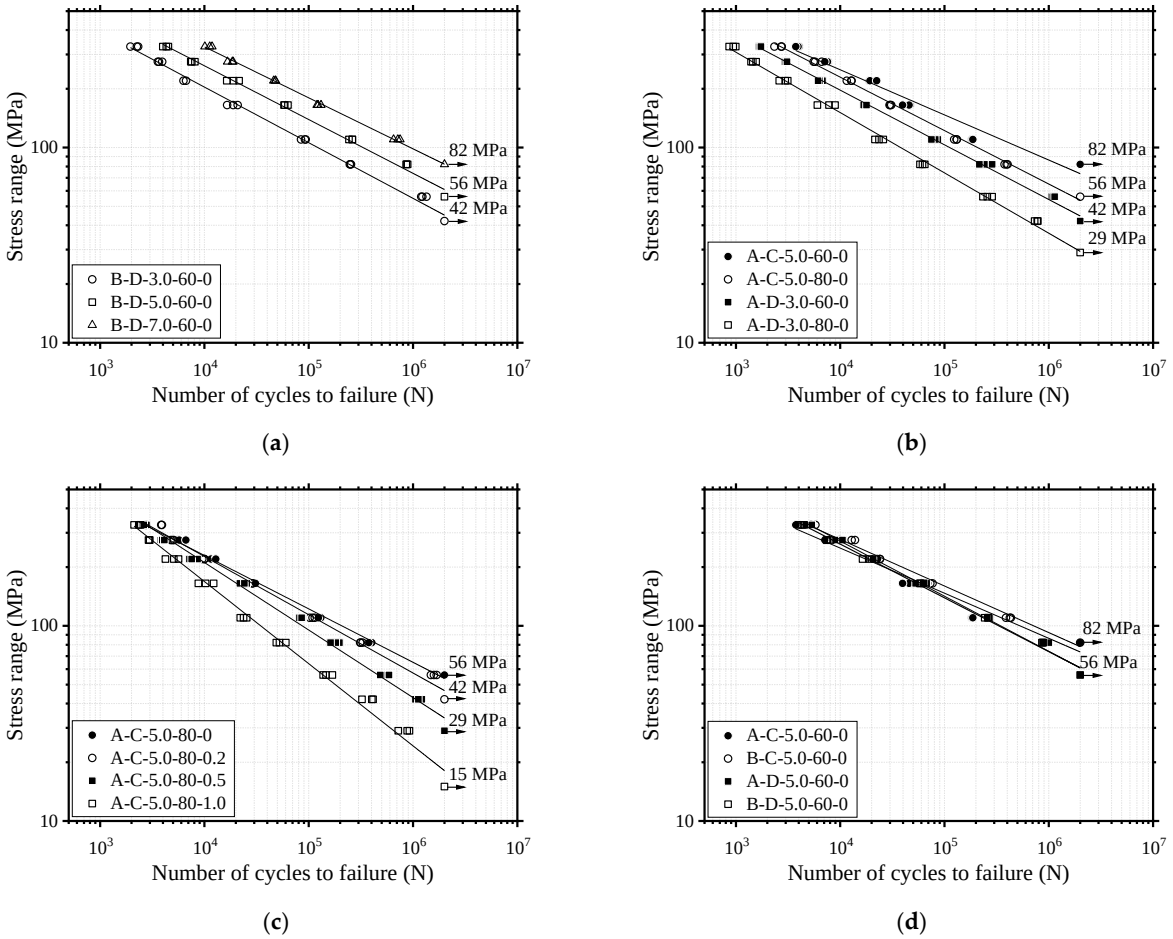

Figure 6. Fatigue behavior of lap joint weld by welding conditions. (**a**) WFR variation (fixed B position, WP: DC, WS: 60 cm/min, gap: 0 mm), (**b**) WS variation (fixed A position, gap: 0 mm), (**c**) gap variation (fixed A position, WP: CMT, WFR: 5.0 m/min, WS: 80 cm/min), and (**d**) position variation (fixed WFR: 5.0 m/min, WS: 60 cm/min, gap: 0 mm).

Using the Basquin model (Equation (1)), BS_M and σ'_{f_M} were derived. M-2SD was applied to the fatigue life at the shared stress range and BS_M and σ'_{f_M} were derived from the logarithmic values in the Basquin model (Equation (4)).

$$log\ \sigma = log\sigma'_{fM} - BS_M \cdot log\ N_f \tag{4}$$

Figure 7 shows BS_M and $log\sigma'_{f_M}$ derived from the S–N curves under varying welding conditions. The X axis represents the deposition rate, which is proportional to WFR and inversely proportional to WS. Figure 7a shows the relationship between the deposition rate and BS_M. As the value of BS_M decreases, the slope of the S–N curve decreases, indicating that the fatigue life increases within the same stress range. The BS_M tends to decrease as the deposition rate increases, regardless of the joint gap size. As the gap of the joint increases, BS_M increases for the same deposition rate. The variation in BS_M was more significant with the joint gap size than the deposition rate. While increasing the deposition rate can reduce BS_M by improving the weld joint's shape, an increase in gap size results in a greater share force acting on the lap joint, thereby degrading the fatigue characteristics of the lap weld. In the field in which chassis parts are manufactured, the joint gap is an uncontrollable variable, so it was not measured separately. It was determined that the weld joint shape measured in Figure 4, including the gap, varies. Figure 7b shows the relationship between

the deposition rate and $log\sigma'_{f_M}$. Although $log\ \sigma'_{f_M}$ did not vary significantly with changes in the deposition rate, it was observed to increase with the increase in the joint gap.

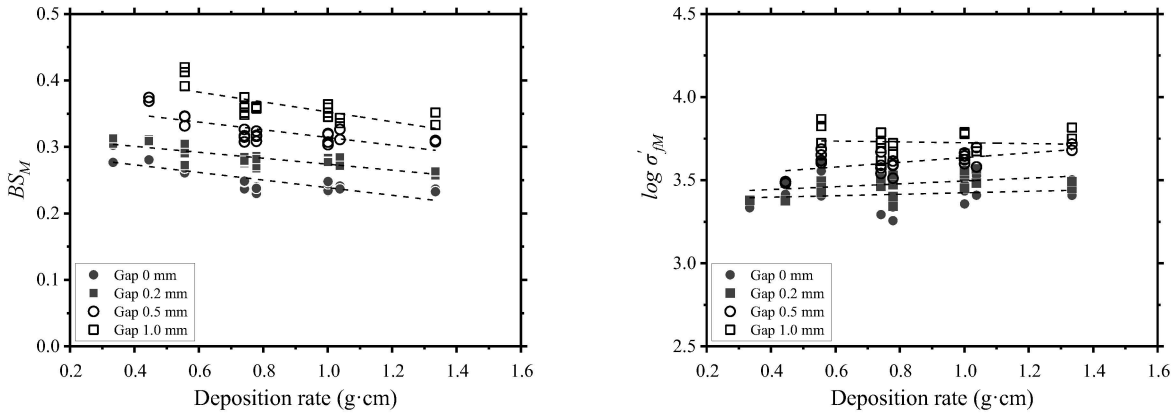

(**a**) (**b**)

Figure 7. The relationship between (**a**) BS_M and (**b**) σ'_{fM} with respect to the deposition rate and gap variation in a lap joint.

σ'_{f_M} is a value derived from the material property in Equation (1), and it has been determined that a verification of changes in the weld joint's properties is necessary. The amount of heat input and colling rate applied to the base material during welding determine changes in the properties of the weld joint, which can be identified through its hardness. The hardness of a weld depends on the amount of heat input, and the formula for calculating the heat input is presented in Equation (5).

$$Heat\ input\left(\frac{J}{cm}\right) = \frac{60 \cdot I \cdot V}{WS} \tag{5}$$

Figure 8 shows the hardness of the weld joint according to variations in heat input and gap. DC and CMT in WP exhibited different current waveform shapes, which led us to anticipate variations in heat input. Welding conditions with the highest and lowest heat input were selected in each WP. The joint position was fixed to the A position, respectively. The heat inputs calculated using average current and voltage, for the welding conditions A-D-3.0-80-0, A-C-5.0-80-1.0, A-D-7.0-60-1.0, and A-C-9.0-60-0, were 1.76, 1.92, 6.52, and 5.29 kJ/cm, respectively.

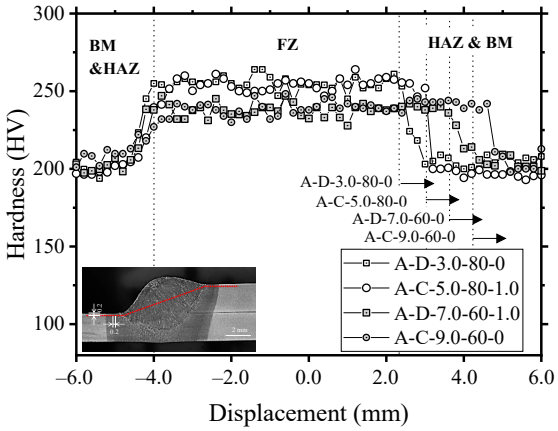

Figure 8. Hardness distribution of the lap weld according to heat input and gap.

The base metal was at 199 HV on average, and HAZ softening was not observed. With the increase in heat input, an increase in the size of FZ and a difference in hardness within

FZ were observed. The hardness of FZ under various welding conditions, A-DC-3-80-0, A-DC-7-60-1.0, A-CMT-5-80-1.0, and A-CMT-9-60-0, was to be 255, 237, 255, and 239 HV, respectively. The difference in heat input resulted in hardness variations, although no hardness difference was observed with a change in the gap size. An increase in heat input delays the solidification of the molten pool, leading to a rise in ferrite structures in the target material's FZ. This increase in ferrite structures, which have a lower hardness compared with bainite and martensite structures, decreases the hardness of the FZ [34]. Kim et al. [35] investigated the fatigue characteristics of lap welds in the subject material; despite the low FZ hardness in the welded joints with high fatigue strength, the fatigue characteristics of the welded joints improved by enhancing the weld shape.

In Figure 7b, variations in $log\ \sigma'_{f_M}$, representing material characteristics, were evident with a change in gap size, whereas differences in $log\ \sigma'_{f_M}$ due to variations in heat input were scarcely observed. Therefore, $log\ \sigma'_{f_M}$ was not adopted as a dependent variable in the prediction model of this study.

5. Fatigue Prediction Model for Statistical Analysis

5.1. Correlation Analysis between the Weld Joint Geometry and Dependent Variables (BS_M, σ_{SFS})

Before conducting regression analysis, a correlation matrix between the dependent (BS_M and σ_{SFS}) and independent (X1–17) variables was computed to determine their relationships. Generally, a higher correlation between predictor variables and dependent variable implies a more significant influence of those predictors on the outcome, which is essential between variables. Therefore, in some cases, variables with strong correlations could still remain inappropriate for inclusion in a regression model if the model assumptions are not met. Conversely, even variables with low correlation coefficients could contribute to reducing the error in a regression model. Additionally, the intercorrelation among independent variables should be considered. High intercorrelation indicates similar impacts of the variables on BS_M and σ_{SFS}, potentially leading to multi-collinearity effects that increase errors in all models.

The correlation analysis was conducted to examine the linearity between dependent and independent variables, and among independent variables. Table 5 illustrates the correlation analysis results of variables concerning BS_M and σ_{SFS}. In the correlation analysis between BS_M and the independent variables, X10 showed a correlation of 0.82, while X14 demonstrated −0.84, indicating a stronger linear relationship with BS_M than other factors. In the correlation analysis between σ_{SFS} and the independent variables, X10 and X14 were observed to exhibit strong linear relationships with correlation coefficients of −0.84 and 0.83, respectively.

Table 5. Correlation matrix between the independent variables and BS_M/σ_{SFS}.

	BS_M	σ_{SFS}	X1	X2	X3	X4	X5	X6	X7	X8	X9	X10	X11	X12	X13	X14	X15	X16
X1	−0.66	0.76																
X2	−0.26	0.51	0.63															
X3	−0.02	0.27	0.54	0.83														
X4	0.62	−0.43	−0.35	0.16	0.49													
X5	−0.77	0.78	0.60	0.36	0.07	−0.46												
X6	0.21	0.07	0.26	0.84	0.89	0.61	−0.13											
X7	−0.13	0.37	0.50	0.74	0.68	0.24	0.22	0.66										
X8	−0.15	0.21	0.06	0.25	0.05	0.04	0.19	0.16	0.29									
X9	−0.73	0.69	0.88	0.27	0.26	−0.56	0.58	−0.13	0.21	−0.11								
X10	0.82	−0.84	−0.75	−0.61	−0.33	0.49	−0.67	−0.18	−0.39	−0.18	−0.66							
X11	0.68	−0.66	−0.90	−0.24	−0.23	0.53	−0.53	0.13	−0.22	0.06	−0.96	0.60						
X12	−0.59	0.59	0.89	0.21	0.19	−0.46	0.45	−0.12	0.22	−0.01	0.86	−0.51	−0.97					
X13	0.79	−0.67	−0.55	−0.07	0.31	0.92	−0.74	0.47	0.04	−0.09	−0.68	0.66	0.63	−0.55				
X14	−0.84	0.83	0.74	0.43	0.09	−0.72	0.77	−0.08	0.22	0.15	0.73	−0.82	−0.69	0.61	−0.86			
X15	−0.58	0.74	0.96	0.80	0.66	−0.23	0.59	0.45	0.62	0.12	0.75	−0.77	−0.75	0.70	−0.45	0.71		
X16	0.38	−0.11	0.11	0.71	0.82	0.70	−0.24	0.95	0.63	0.11	−0.24	0.03	0.22	−0.20	0.60	−0.23	0.29	
X17	−0.07	0.33	0.47	0.80	0.76	0.31	0.16	0.77	0.98	0.27	0.15	−0.39	−0.16	0.15	0.12	0.18	0.62	0.74

The correlation analysis among independent variables revealed significant correlations, with a correlation coefficient of 0.96 between X1 and X15, 0.95 between X6 and X16, 0.98 between X7 and X17, −0.96 between X9 and X11, and −0.97 between X11 and X12. Such high correlation values indicate strong relationships among the variables, and caution should be exercised when including them in the regression model. The regression model used the remaining factors, excluding X6, X11, X12, X15, and X17, with correlation coefficients exceeding 0.95 among the independent variables.

5.2. Regression Model for S–N Curve Prediction

The selected weld shape parameters were normalized and used as independent variables. Multi-linear regression analysis was conducted using the backward elimination method, a technique employed in regression analysis to simplify models by iteratively removing non-significant variables based on their *p*-value. Furthermore, the approach allows for a more interpretable model and assists in preventing overfitting.

The variables were systematically eliminated from the regression model based on the criteria of partial correlation coefficients and the significance level of regression coefficients with a threshold of 0.05. The accuracy of the regression model was assessed using the adjusted coefficient of determination and the standard error of the estimates. The adjusted coefficient of determination was particularly valuable as it accounted for model complexity and is often preferred over traditional coefficients. Equations (6)–(8) were used to represent the coefficient of determination, adjusted coefficient of determination, and standard error of the estimates, respectively.

$$R^2 = 1 - \frac{\sum_{i=1}^{n} (y_i - \hat{y}_i)^2}{\sum_{i=1}^{n} (y_i - \overline{y})^2} \tag{6}$$

$$R^2_{adj} = 1 - \left(1 - R^2\right) \cdot \frac{n-1}{n-k-1} \tag{7}$$

$$SE(\varepsilon) = \frac{\sqrt{\Sigma (\hat{y}_\mathrm{i} - y_\mathrm{i})^2}}{n-k-1} \tag{8}$$

where n denotes the number of samples, k represents the number of independent variables, y_i is the i-th actual measurement data, $\hat{y}_i$ is the predicted value for the i-th data point, and $\overline{y}$ represents the mean value of the dependent variable y.

Table 6 presents the backward elimination regression analysis results for *Model* I_{BS_M}. A total of eight steps were performed, and the variables X7, X13, X2, X3, X8, X1, and X5 were removed in higher order of their *p*-values, which exceeded 0.05. Despite reducing the number of independent variables, R^2_{adj} remained unchanged at 0.86 and the final $SE(\varepsilon)$ value was 0.170, the same as it was in step 1. Therefore, the model from step 8 was presented as the final regression equation for predicting BS_M using linear multiple regression analysis. Table 7 presents the regression analysis results obtained using the backward elimination method for *Model* $I_{\sigma_{SFS}}$, which followed the same procedure as BS_M. A total of eight steps resulted in removing variables in the following order: X13, X8, X9, X3, X2, X5, and X1. After eight steps, R^2_{adj} remained at 0.838, and $SE(\varepsilon)$ was 7.461. Accordingly, the regression model is represented as Equation (9).

$$\begin{aligned} \textit{Model } I_{BS_M} &= 3.326 - 0.86X4 - 0.26X9 + 0.90X10 - 0.85X14 + 1.00X16 \\ \textit{Model } I_{\sigma_{SFS}} &= -47.9 + 51.44X4 + 17.40X7 - 28.72X10 + 54.70X14 - 36.03X16 \end{aligned} \tag{9}$$

The variables X4, X10, X14, and X16 were observed to simultaneously satisfy the significance level of 0.05 for both BS_M and σ_{SFS}. The standardized regression coefficient was utilized to examine the contributions of the variables used to determine the fatigue characteristics. The contributions are presented in Table 8. The standardized regression coefficients revealed that X14 had the most significant influence, followed by X4, X10, X16,

and X9 as the critical factors for predicting BS_M. For σ_{SFS}, the order of importance for factors was X14, X4, X10, X16, and X7.

Table 6. Significance provability values of regression coefficients for the back elimination method and its result for *Model* I_{BS_M}.

p-Value	Step							
	#1	**#2**	**#3**	**#4**	**#5**	**#6**	**#7**	**#8**
X1	0.20	0.20	0.21	0.16	0.11	0.18	-	-
X2	0.73	0.74	0.83	-	-	-	-	-
X3	0.35	0.34	0.33	0.29	-	-	-	-
X4	0.07	0.06	0.01	0.00	0.00	0.00	0.00	0.00
X5	0.24	0.24	0.19	0.11	0.10	0.09	0.14	-
X7	0.83	-	-	-	-	-	-	-
X8	0.26	0.23	0.24	0.23	0.19	-	-	-
X9	0.05	0.05	0.04	0.01	0.01	0.03	0.03	0.03
X10	0.00	0.00	0.00	0.00	0.00	0.00	0.00	0.00
X13	0.075	0.76	-	-	-	-	-	-
X14	0.00	0.00	0.00	0.00	0.00	0.00	0.00	0.00
X16	0.11	0.10	0.11	0.08	0.00	0.00	0.00	0.00
R^2_{adj}	0.86	0.86	0.86	0.86	0.86	0.86	0.86	0.86
$SE(\varepsilon)$	0.170	0.169	0.168	0.167	0.167	0.167	0.169	0.170

Table 7. Significance provability values of regression coefficients for the back elimination method and its result for *Model* $I_{\sigma_{SFS}}$.

p-Value	Step							
	#1	**#2**	**#3**	**#4**	**#5**	**#6**	**#7**	**#8**
X1	0.62	0.61	0.60	0.24	0.10	0.07	0.07	-
X2	0.59	0.53	0.52	0.52	0.53	-	-	-
X3	0.78	0.74	0.73	0.83	-	-	-	-
X4	0.02	0.00	0.00	0.00	0.00	0.00	0.00	0.00
X5	0.37	0.25	0.24	0.20	0.18	0.09	-	-
X7	0.10	0.09	0.08	0.08	0.06	0.06	0.03	0.01
X8	0.97	0.97	-	-	-	-	-	-
X9	0.80	0.78	0.78	-	-	-	-	-
X10	0.01	0.00	0.01	0.00	0.00	0.00	0.00	0.00
X13	0.98	-	-	-	-	-	-	-
X14	0.00	0.00	0.00	0.00	0.00	0.00	0.00	0.00
X16	0.23	0.02	0.02	0.02	0.10	0.00	0.00	0.00
R^2_{adj}	0.84	0.84	0.84	0.84	0.85	0.85	0.84	0.84
$SE(\varepsilon)$	7.474	7.424	7.375	7.331	7.286	7.258	7.348	7.461

Table 8. Standardized regression coefficients of Model I.

	X4	**X7**	**X9**	**X10**	**X14**	**X16**
Model I_{BS_M}	−0.50	-	−0.14	0.50	−0.50	0.40
Model $I_{\sigma_{SFS}}$	0.50	0.14	-	−0.38	0.66	−0.36

Another regression model was considered for predicting fatigue characteristics, utilizing the same dependent and independent variables. The non-linear regression model

involved taking the logarithm of the 17 variables extracted from the welded geometry for analysis and back-transforming them to obtain a form similar to Equation (10).

$$Y = \beta_0 \cdot X1^{\beta_1} \cdot X2^{\beta_2} \cdot X3^{\beta_3} \cdot X4^{\beta_4} \cdot \cdots X17^{\beta_{17}} \tag{10}$$

As revealed during the examination of the linear regression model that considered issues including model overfitting and complexity, backward elimination proved to be more effective in constructing the regression model. Therefore, only the results obtained through the method were considered for the non-linear regression model. The results are presented in Equation (11).

$$\begin{aligned} Model\ II_{BS_M} &= 10.23 \cdot X4^{-0.46} \cdot X10^{0.42} \cdot X13^{-0.38} \cdot X14^{-0.35} \cdot X16^{0.44} \\ Model\ II_{\sigma_{SFS}} &= 0.000995 \cdot X3^{-0.72} \cdot X4^{1.04} \cdot X9^{0.78} \cdot X10^{-1.04} \cdot X14^{2.02} \cdot X16^{1.87} \end{aligned} \tag{11}$$

Among the critical factors in the non-linear regression model for predicting BS_M and σ_{SFS}, X4, X10, X14, and X16 were significant in both prediction models. R^2_{adj} for $Model\ II_{BS_M}$ and $Model\ II_{\sigma_{SFS}}$ in the multiple non-linear regression model was 0.863 and 0.860, respectively. Additionally, $SE(\varepsilon)$ values were 0.024 and 0.071, respectively.

The standardized regression coefficients were calculated for *Model II*, a non-linear regression model, using the same method as *Model I* to examine the influence of independent variables on the dependent variable. These results are presented in Table 9. In both $Model\ II_{BS_M}$ and $Model\ II_{\sigma_{SFS}}$, the standardized regression coefficients for X4 and X16 were highest. It was observed that the independent variables X4, X10, X14, and X16 intersect in the non-linear models predicting BS_M and σ_{SFS}. Based on the standardized coefficients of the multi linear regression model and non-linear regression model, which predict the S–N curve (BS_M and σ_{SFS}) through weld geometry factors (independent variables) in a lap weld, it was determined that weld geometry factors X4, X10, X14, and X16 are significant variables.

Table 9. Standardized regression coefficients of *Model II*.

	X3	X4	X9	X10	X13	X14	X16
$Model\ II_{BS_M}$	-	−0.518	-	0.483	−0.372	−0.409	0.458
$Model\ II_{\sigma_{SFS}}$	−0.237	0.365	0.287	−0.408	-	0.781	0.785

Finally, a second-order polynomial regression model was applied to predict BS_M and σ_{SFS}. Considering complexity and analysis, only four independent variables (X4, X10, X14, X16) were used, and backward elimination was applied to enhance the model performance, as shown in Equation (12).

$$\begin{aligned} Model\ III_{BS_M} &= 3.02 + 0.97X4 + 0.94X10 - 1.08X14 - 1.01X16 - 1.07X4^2 + 1.25X14 \cdot X16 \\ Model\ III_{\sigma_{SFS}} &= 491 - 624X4 - 26.27X10 - 464X14 + 491X16 + 142.4X4^2 + 112.6X14^2 + 291.4X \cdot X14 \\ &\quad -145.9X14 \cdot X16 - 186X14 \cdot X16 \end{aligned} \tag{12}$$

The regression analysis showed that the R^2_{adj} values for $Model\ III_{BS_M}$, and $Model\ III_{\sigma_{SFS}}$ were 0.863 and 0.851, respectively. The values of $SE(\varepsilon)$ were 0.168 and 7.158, respectively. Although the second-order polynomial regression model introduced a more complex structure, compared with the multiple linear and non-linear models, the coefficient of determination and standard error were not improved.

Various regression analyses were employed to statistically analyze the impact of weld joint geometry on fatigue characteristics and propose diverse fatigue property prediction models. While slight variations did exist among the models used, up to 86% of the total variability could be explained collectively. Figure 9 compares the measured and predicted values of BS_M and σ_{SFS}, with the quantified results presented in Tables 10 and 11.

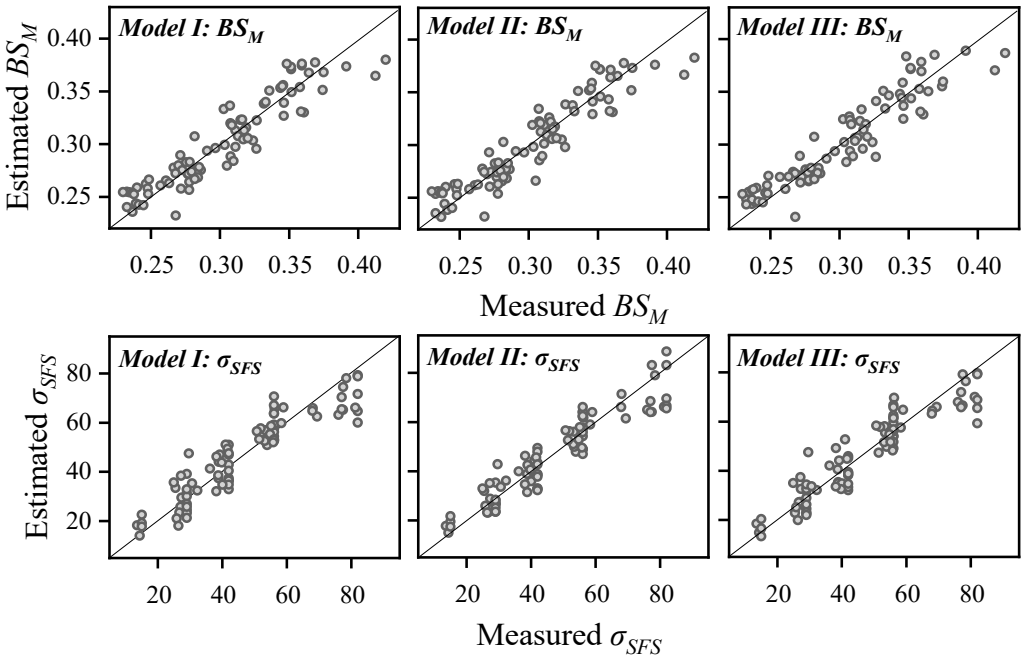

Figure 9. Relationship between measured value and estimated value by regression models.

Table 10. Coefficient of determination and standard error of the estimate for the BS_M estimation models.

BS_M	*Model I*	*Model II*	*Model III*
R^2_{adj}	0.863	0.867	0.863
$SE(\varepsilon)$	0.170	0.024	0.168

Table 11. Coefficient of determination and standard error of the estimate for the σ_{SFS} estimation models.

σ_{SFS}	*Model I*	*Model II*	*Model III*
R^2_{adj}	0.838	0.860	0.851
$SE(\varepsilon)$	7.461	0.071	7.158

5.3. Fatigue Life Prediction Using Statistical Models

BS_M and σ_{SFS} were derived using the *Basquin eqation* and predicted through statistical modeling. Measuring the weld size allowed for the prediction of the slope of the S–N curve and the endurance limit (2×10^6 cycles). In this study, we aim to predict the fatigue characteristics of chassis components by determining fatigue and endurance limits for automobile chassis parts. The chassis comprise various components, and the magnitude and nature of stress were confirmed to vary depending on these components. In evaluating the fatigue life of chassis components, durability assessments were conducted by maintaining a constant load control value rather than assessing the component fatigue life based on fatigue load variations, as typically undertaken when deriving the S–N curve. Thus, a minimum fatigue life of 100,000–300,000 cycles was required. As a result, predicting fatigue life through weld configuration and fatigue stress could assist in assessing the fatigue characteristics of chassis components.

The main derived factors (X4, X10, X14, X16) and the applied stress (σ_r) were selected as independent variables, while fatigue life was designated as the dependent variable. A regression model for predicting fatigue life was developed using the backward elimination method. Equations (13)–(15) represent the results of regression models for predicting fatigue

life, including multiple linear (*Model IV*), multiple non-linear (*Model V*), second-order polynomial (*Model VI*) models.

$$Model\ IV: logN = 4.257 - 0.01\sigma_r + 0.71X4 - 0.34X10 + 0.96X14 \quad (13)$$

$$Model\ V: N = 6.19 \cdot \sigma_r^{-3.10} \cdot X4^{2.39} \cdot X10^{-1.64} \cdot X14^{3.59} \quad (14)$$

$$\begin{aligned} Model\ VI: N = {} & 17.46 - 0.01\sigma_r - 7.63X4 - 4.96X10 - 9.87X14 + 6.40X16 + 1.90X4^2 + 0.77X10^2 \\ & + 2.06X14^2 + 3.55X4 \cdot X14 - 1.96X4 \cdot X16 + 1.60X10 \cdot X14 - 2.18X14 \cdot X16 \end{aligned} \quad (15)$$

Table 12 presents the results of regression analysis. The R^2_{adj} value for *Model V* was the highest at 0.955. *Model IV* and *Model VI* had R^2_{adj} value of 0.904 and 0.906, respectively. Furthermore, the $SE(\varepsilon)$ value for *Model IV*, *Model V*, and *Model VI* were 0.301, 0.206, and 0.299, respectively. With the highest R^2_{adj} and lowest $SE(\varepsilon)$ values, *Model V* proved superior for predicting fatigue life among the models. The results of predicting fatigue life based on these load and key factor variables are presented in Figure 10.

Table 12. Coefficient of determination and standard error of the estimate for the *N* estimation models.

N	*Model IV*	*Model V*	*Model VI*
R^2_{adj}	0.904	0.955	0.906
$SE(\varepsilon)$	0.301	0.206	0.299

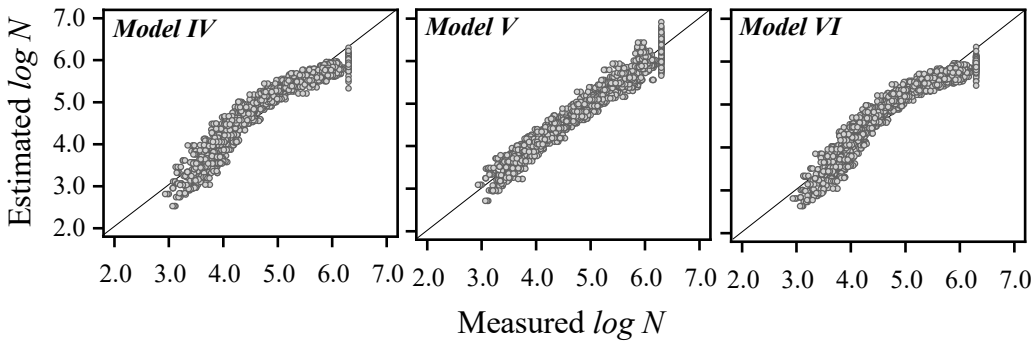

Figure 10. Relationship between measured number of cycles to failure (log*N*) and estimated number of cycles to failure (log*N*) by regression model.

5.4. Analysis of Significant Weld Geometry Affecting Fatigue Characteristics

X4, X10, X14, and X16 were considered significant factors in predicting fatigue behavior for lap welds that include a gap. Fatigue fracture in lap joints occurs in two forms [36]. In one case, a fatigue crack initiates at the weld toe on the top surface of the bottom plate and propagates to the bottom surface of the bottom plate, leading to failure (Figure 11a). In the other case, a fatigue crack initiates at the weld root and propagates to the top surface of the top plate, resulting in failure (Figure 11b). Figure 12 illustrates a schematic of the stress distribution at area A (σ_A), B (τ_B), C (τ_c) when subjected to tensile forces in lap welds [37]. During load application, stress distribution in the weld joint was not uniform (Figure 12a). Herein, t represents the material thickness (2.3 mm) and l denotes the width of the fatigue specimen (10 mm). The same stress acted in area A, where thickness and width were uniform (Equation (16)). The force acting on area B resulted in shear stress (τ_B); and, as X4 increased, τ_B decreased (Equation (17)). Finally, at area C, stress concentration was the greatest at the red point on the bottom plate, and an increase in angle X10 led to an increase in shear stress on the welded toe surface of the bottom plate (Equation (18)). The additional bending stress occurred at the joint in tension due to the eccentricity between one-side lap welds and the applied force, as depicted in Figure 12b.

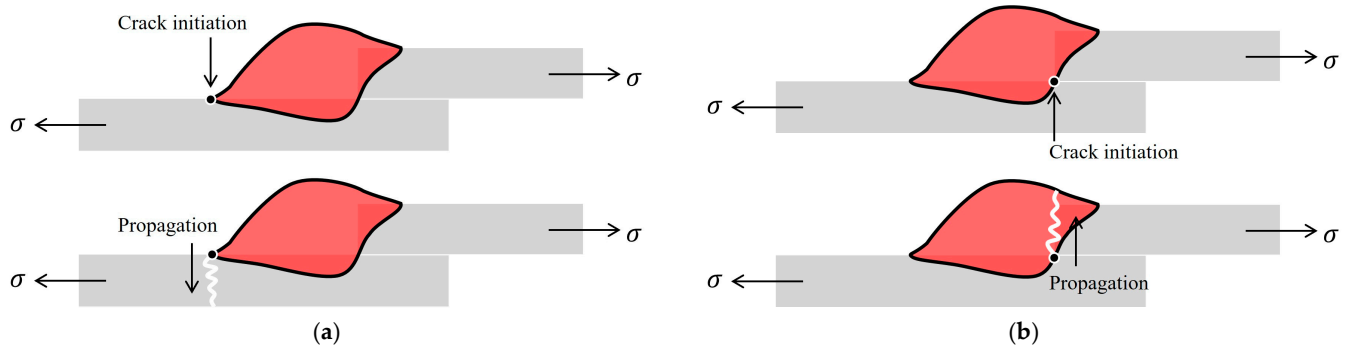

Figure 11. Schematic of fatigue fracture in lap joint welds. (**a**) Weld toe fracture and (**b**) weld root fracture.

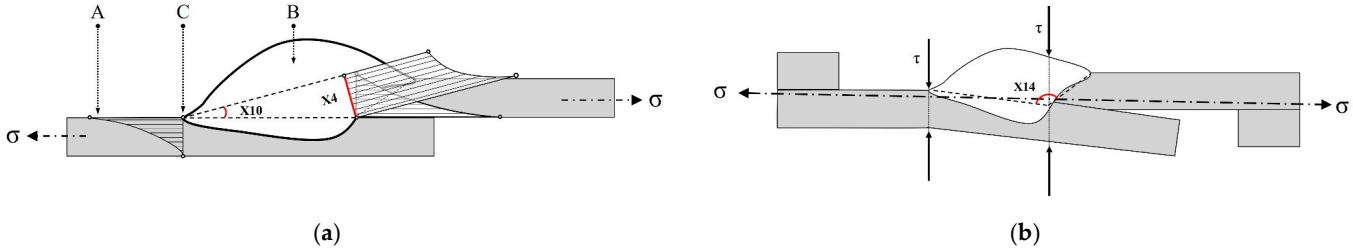

Figure 12. Stress distribution of lap welds during loading. (**a**) Stress distribution field and (**b**) bending morphology at weld toe and root stress concentration.

The higher the stress, the greater the bending force, thereby increasing stress concentration at the weld root. Therefore, the magnitude of X14 was considered to be crucial. Additionally, the magnitude of X16 was expected to be determined by X4, X10, and X14. In conclusion, the four factors (X4, X10, X14, and X16) derived from the regression model can be considered as variables that represent stress concentration and magnitude in the lap welds, allowing us to predict fatigue characteristics.

$$\sigma_A = \frac{F}{A_1} = \frac{F}{t \cdot l} \tag{16}$$

$$\tau_B = \frac{F}{A_2} = \frac{F}{X4 \cdot l} \tag{17}$$

$$\tau_c = \frac{F}{cos\theta d\theta} = F \cdot sec\theta tan\theta = F \cdot \frac{sin\theta}{cos^2\theta} \tag{18}$$

6. Conclusions

In this study, we developed a statistical analysis-based model to predict the fatigue characteristics of lap welds using the weld geometry factors of lap joints and proposed key weld geometry factors in response to the fatigue characteristics of welds with gaps.

(1) A GA590 2.3 mm sheets were overlapped, and welding performed by varying the joint position, WP, WFR, WS, and gap to produce various weld geometries. Among the weld geometry factors, the size of seven length factors, including leg length; seven angle factors, including toe angle; and three area factors, were measured and utilized as independent variables to predict fatigue characteristics.

(2) Eighty-seven S–N curves were derived under various welding conditions, and the S–N curves varied according to change in WP, gap size, WFR, and WS. The Basuin equation determined the BS_M and $\sigma'_{f\,M}$ for each S–N curve. The BS_M increased with the gap size and showed a decreasing trend as the deposition rate increased. The $\sigma'_{f\,M}$

showed a slight upward trend with increasing gap size, while significant changes were not observed with variations in the deposition rate.

(3) BS_M and σ_{SFS} were selected as dependent variables to predict the S–N curve with the M-2SD applied, and 17 weld geometry factors were used as independent variables. Through correlation analysis, the weld geometry factors X6, X11, X12, X15, and X17, which showed multicollinearity among variables, were excluded from the independent variables.

(4) Backward elimination was applied to develop multiple linear and non-linear regression models to predict BS_M and σ_{SFS}. The weld geometry factors applied across both multiple linear regression models and multiple non-linear regression models were X4 (length), X10 (Angle), X14 (Area), and X16 (Area). Upon examining the standardized regression coefficients, the four factors were identified as the primary weld geometry factors for predicting BS_M and σ_{SFS}.

(5) For the multiple linear regression model, the adjusted R-squared values for BS_M and σ_{SFS} were 0.863 and 0.838, respectively. The adjusted R-squared values for the multiple non-linear regression models for BS_M and σ_{SFS} were 0.867 and 0.860, respectively. The second-order polynomial regression model performed backward elimination on the four significant weld geometry factors, resulting in adjusted R-squared values of 0.863 and 0.851 for BS_M and σ_{SFS}, respectively. The predictive performance of the three regression models was nearly identical at around 86%, but the multiple non-linear regression model showed slightly better performance.

(6) A statistical model for predicting fatigue life based on the key weld geometry factors was proposed. The adjusted R-squared and standard error of the estimates for the multiple non-linear regression model were 0.955 and 0.206, respectively, confirming its excellent predictive performance in estimating fatigue life.

(7) Among the weld geometry factors of the lap joint with a gap, X4, X10, X14, and X16 are considered to be closely related to stress concentration. These four factors are judged to predict fatigue characteristics.

When manufacturing chassis components that are subject to fatigue loading, it is challenging to completely eliminate or consistently manage the gap. Aspects such as leg length, penetration depth, throat thickness, and the toe angle of the weld in lap joint are managed in the manufactured chassis components. The controlled weld geometry remains the same even if a gap occurs in the lap joint. For lap joints with gaps that require fatigue characteristics, it is necessary to manage new weld geometry factors such as X10, X14, and X16, in addition to throat thickness (X4).

Additionally, easy statistical analysis of the main weld geometry factors predicting fatigue characteristics in lap joints, which requires significant time and cost, is possible.

Author Contributions: Conceptualization, J.Y.; Methodology, D.-Y.K. and J.Y.; Validation, J.Y.; Formal analysis, D.-Y.K. and J.Y.; Investigation, D.-Y.K.; Resources, J.Y.; Data curation, D.-Y.K.; Writing—original draft, D.-Y.K.; Writing—review & editing, J.Y.; Visualization, D.-Y.K.; Supervision, J.Y.; Project administration, J.Y.; Funding acquisition, J.Y. All authors have read and agreed to the published version of the manuscript.

Funding: This research was supported by the 2024 Ministry of Trade, Industry and Energy and the Korea Planning and Evaluation Institute of Industrial Technology (KEIT) grant funding (Development of mechanical joining systems and smart joining lines for assembly of electric vehicle chassis and battery case, 20022489, Ministry of Trade, Industry and Energy).

Data Availability Statement: The original contributions presented in the study are included in the article, further inquiries can be directed to the corresponding author.

Acknowledgments: Special thanks are extended to Moonjin Kang for conducting the research project together and providing insightful comments on the experimental observations.

Conflicts of Interest: The authors declare no conflict of interest.

Appendix A

Table A1. Fatigue combination for case study.

	Joint	WP	WFR	WS	Gap		Joint	WP	WP	WS	Gap
A-C-5.0-60-0	A	CMT	5.0	60	0	A-C-5.0-80-0	A	CMT	5.0	80	0
A-C-7.0-60-0	A	CMT	7.0	60	0	A-C-7.0-80-0	A	CMT	7.0	80	0
A-C-9.0-60-0	A	CMT	9.0	60	0	A-C-9.0-80-0	A	CMT	9.0	80	0
A-C-5.0-60-0.2	A	CMT	5.0	60	0.2	A-C-5.0-80-0.2	A	CMT	5.0	80	0.2
A-C-7.0-60-0.2	A	CMT	7.0	60	0.2	A-C-7.0-80-0.2	A	CMT	7.0	80	0.2
A-C-9.0-60-0.2	A	CMT	9.0	60	0.2	A-C-9.0-80-0.2	A	CMT	9.0	80	0.2
A-C-5.0-60-0.5	A	CMT	5.0	60	0.5	A-C-5.0-80-0.5	A	CMT	5.0	80	0.5
A-C-7.0-60-0.5	A	CMT	7.0	60	0.5	A-C-7.0-80-0.5	A	CMT	7.0	80	0.5
A-C-9.0-60-0.5	A	CMT	9.0	60	0.5	A-C-9.0-80-0.5	A	CMT	9.0	80	0.5
A-C-5.0-60-1.0	A	CMT	5.0	60	1.0	A-C-5.0-80-1.0	A	CMT	5.0	80	1.0
A-C-7.0-60-1.0	A	CMT	7.0	60	1.0	A-C-7.0-80-1.0	A	CMT	7.0	80	1.0
A-C-9.0-60-1.0	A	CMT	9.0	60	1.0	A-C-9.0-80-1.0	A	CMT	9.0	80	1.0
A-D-3.0-60-0	A	DC	3.0	60	0	A-D-3.0-80-0	A	DC	3.0	80	0
A-D-5.0-60-0	A	DC	5.0	60	0	A-D-5.0-80-0	A	DC	5.0	80	0
A-D-7.0-60-0	A	DC	7.0	60	0	A-D-7.0-80-0	A	DC	7.0	80	0
A-D-3.0-60-0.2	A	DC	3.0	60	0.2	A-D-5.0-80-0.2	A	DC	5.0	80	0.2
A-D-5.0-60-0.2	A	DC	5.0	60	0.2	A-D-7.0-80-0.2	A	DC	7.0	80	0.2
A-D-7.0-60-0.2	A	DC	7.0	60	0.2	A-D-5.0-80-0.5	A	DC	5.0	80	0.5
A-D-3.0-60-0.5	A	DC	3.0	60	0.5	A-D-7.0-80-0.5	A	DC	7.0	80	0.5
A-D-5.0-60-0.5	A	DC	5.0	60	0.5	A-D-5.0-80-1.0	A	DC	5.0	80	1.0
A-D-7.0-60-0.5	A	DC	7.0	60	0.5	A-D-7.0-80-1.0	A	DC	7.0	80	1.0
A-D-5.0-60-1.0	A	DC	5.0	60	1.0						
A-D-7.0-60-1.0	A	DC	7.0	60	1.0						
B-C-5.0-60-0	B	CMT	5.0	60	0	B-C-5.0-80-0	B	CMT	5.0	80	0
B-C-7.0-60-0	B	CMT	7.0	60	0	B-C-7.0-80-0	B	CMT	7.0	80	0
B-C-9.0-60-0	B	CMT	9.0	60	0	B-C-9.0-80-0	B	CMT	9.0	80	0
B-C-5.0-60-0.2	B	CMT	5.0	60	0.2	B-C-5.0-80-0.2	B	CMT	5.0	80	0.2
B-C-7.0-60-0.2	B	CMT	7.0	60	0.2	B-C-7.0-80-0.2	B	CMT	7.0	80	0.2
B-C-9.0-60-0.2	B	CMT	9.0	60	0.2	B-C-9.0-80-0.2	B	CMT	9.0	80	0.2
B-C-5.0-60-0.5	B	CMT	5.0	60	0.5	B-C-5.0-80-0.5	B	CMT	5.0	80	0.5
B-C-7.0-60-0.5	B	CMT	7.0	60	0.5	B-C-7.0-80-0.5	B	CMT	7.0	80	0.5
B-C-9.0-60-0.5	B	CMT	9.0	60	0.5	B-C-9.0-80-0.5	B	CMT	9.0	80	0.5
B-C-5.0-60-1.0	B	CMT	5.0	60	1.0	B-C-5.0-80-1.0	B	CMT	5.0	80	1.0
B-C-7.0-60-1.0	B	CMT	7.0	60	1.0	B-C-7.0-80-1.0	B	CMT	7.0	80	1.0
B-C-9.0-60-1.0	B	CMT	9.0	60	1.0	B-C-9.0-80-1.0	B	CMT	9.0	80	1.0
B-D-3.0-60-0	B	DC	3.0	60	0	B-D-3.0-80-0	B	DC	5.0	80	0
B-D-5.0-60-0	B	DC	5.0	60	0	B-D-5.0-80-0	B	DC	7.0	80	0
B-D-7.0-60-0	B	DC	7.0	60	0	B-D-7.0-80-0	B	DC	9.0	80	0
B-D-3.0-60-0.2	B	DC	3.0	60	0.2	B-D-3.0-80-0.2	B	DC	3.0	80	0.2
B-D-5.0-60-0.2	B	DC	5.0	60	0.2	B-D-5.0-80-0.2	B	DC	5.0	80	0.2
B-D-7.0-60-0.2	B	DC	7.0	60	0.2	B-D-7.0-80-0.2	B	DC	7.0	80	0.2
B-D-3.0-60-0.5	B	DC	3.0	60	0.5	B-D-5.0-80-0.5	B	DC	5.0	80	0.5
B-D-5.0-60-0.5	B	DC	5.0	60	0.5	B-D-7.0-80-0.5	B	DC	7.0	80	0.5
B-D-7.0-60-0.5	B	DC	7.0	60	0.5						
B-D-5.0-60-1.0	B	DC	5.0	60	1.0						
B-D-7.0-60-1.0	B	DC	7.0	60	1.0						

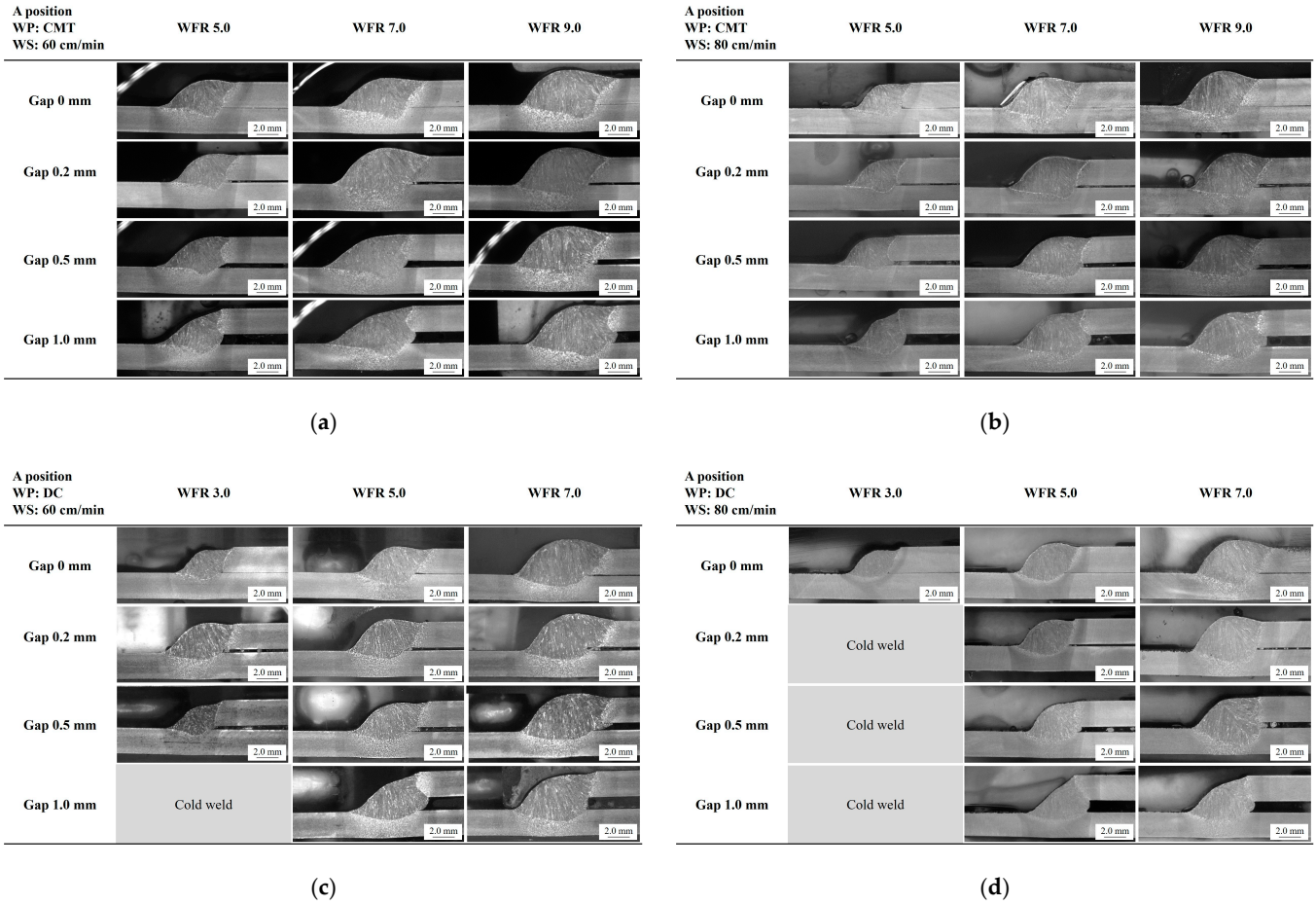

Figure A1. Cross-sectional images of the weld according to the welding parameters at position A: (**a**) WP: CMT, WS: 60 cm/min; (**b**) WP: CMT, WS: 80 cm/min; (**c**) WP: DC, WS: 60 cm/min; and (**d**) WP: DC, WS: 80 cm/min.

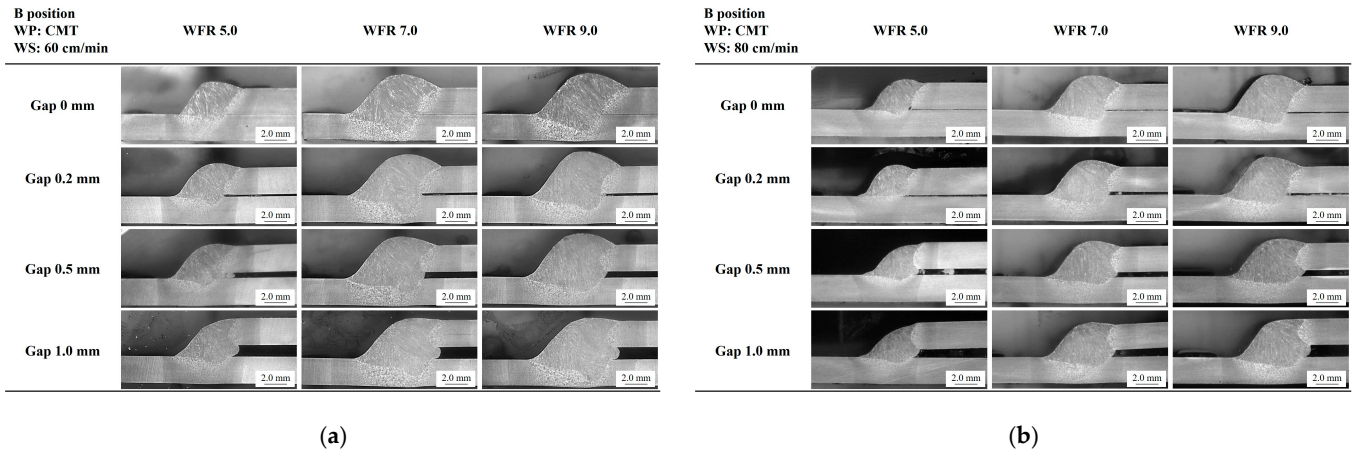

Figure A2. *Cont*.

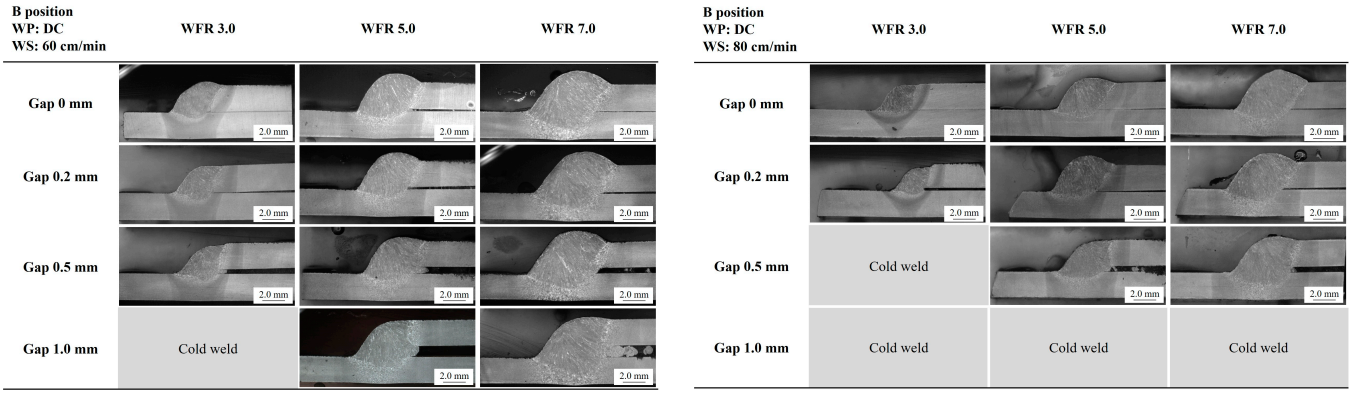

(**c**) (**d**)

Figure A2. Cross-sectional images of the weld according to the welding parameters at position B: (**a**) WP: CMT, WS: 60 cm/min; (**b**) WP: CMT, WS: 80 cm/min; (**c**) WP: DC, WS: 60 cm/min; (**d**) and WP: DC, WS: 80 cm/min.

References

1. Suzuki, R.; Kasai, R. Expansion of "MX-MIG process" as pure argon gas shielded welding method-for carbon steel. *Kobelco Technol. Rev.* **2013**, *32*, 24–32.
2. Yoshitake, A.; Kinoshita, M.; Osawa, K.; Ogawa, K.; Nakagawa, H.; Kabasawa, M. Fatigue properties of fillet welded lap joints of high strength steel sheets for automobiles. *SAE Trans.* **1994**, *103*, 142–147.
3. Bae, G.; Jeong, H. Development trend and prospect for improving fatigue performance of advanced high strength steel welds in automotive chassis applications. *J. Weld. Join.* **2017**, *35*, 17–27. [CrossRef]
4. Ahiale, G.K.; Oh, Y.J.; Choi, W.D.; Lee, K.B.; Jung, J.G.; Nam, S.W. Microstructure and fatigue resistance of high strength dual phase steel welded with gas metal arc welding and plasma arc welding processes. *Met. Mater. Int.* **2013**, *19*, 933–939. [CrossRef]
5. El-Batahgy, A.M. Influence of HAZ microstructure and stress concentration on fatigue strength of welded structural steel. *Mater. Lett.* **1994**, *21*, 415–423. [CrossRef]
6. Koganti, R.; Angotti, S.; Joaquin, A.; Jiang, C.C. *Effect of Weld Geometry and HAZ Softening on Fatigue Performance of DP780 GMAW Lap Joint*; SAE Technical Paper 2007-01-0632; Society of Automotive Engineers Inc.: Warrendale, PA, USA, 2007.
7. Chung, Y.; Kwon, H. A Study on weld fatigue life improvement of automotive chassis components. In Proceedings of the KSME 2011 Autumn Annual Meeting, Daegu, Republic of Korea, 2–4 November 2011; The Korean Society of Mechanical Engineers: Seoul, Republic of Korea, 2011; pp. 129–132.
8. Feng, Z.; Sang, Y.; Jiang, C.; Chiang, J.; Kuo, M. *Fatigue Performance of Advanced High-Strength Steels (AHSS) GMAW Joints*; SAE Technical Paper 2009-01-0256; Society of Automotive Engineers Inc.: Warrendale, PA, USA, 2009.
9. Lee, K.B.; Oh, S.T. Development of durability enhancement technology for arc weldings in advanced high strength steel (AHSS) chassis parts. *J. Weld. Join.* **2015**, *33*, 50–56.
10. Duchet, M.; Haouas, J.; Gibeau, E.; Pechenot, F.; Honecker, C.; Munier, R.; Weber, B. Improvement of the fatigue strength of welds for lightweight chassis application made of Advanced High Strength Steels. *Procedia Struct. Integr.* **2019**, *19*, 585–594. [CrossRef]
11. Kodama, S.; Ishida, Y.; Furusako, S.; Saito, M.; Miyazaki, Y.; Nose, T. Arc welding technology for automotive steel sheets. *Nippon Steel Tech. Rep.* **2013**, *103*, 83–90.
12. Kodama, S.; Ishida, Y.; Matsuda, K.; Ogawa, M. Improvement of fatigue strength of arc welded joints using high strength steel sheets for automobile chassis members. *Nippon Steel Tech. Rep.* **2018**, *119*, 59–68.
13. Kim, J.; Lee, K.; Lee, B. Estimation of the fatigue life according to lap joint weld profiles for ferritic stainless steel. *Procedia Eng.* **2011**, *10*, 1979–1984. [CrossRef]
14. Kim, D.Y.; Kim, G.G.; Yu, J.; Kim, D.C.; Kim, Y.M.; Park, J. Weld fatigue behavior of gas metal arc welded steel sheets based on porosity and gap size. *Int. J. Adv. Manuf. Tech.* **2023**, *124*, 1141–1153. [CrossRef]
15. Palmgren, A. Durability of ball bearings. *Z. Vereines Dtsch. Ingenieure* **1924**, *68*, 339–341.
16. Miner, M.A. Cumulative damage in Fatigue. *J. Appl. Mech.* **1945**, *12*, A159–A164. [CrossRef]
17. Fatemi, A.; Yang, L. Cumulative fatigue damage and life prediction theories: A survey of the state of the art for homogeneous materials. *Int. J. Fatigue* **1998**, *20*, 9–34. [CrossRef]
18. Hectors, K.; De Waele, W. Cumulative damage and life prediction models for high-cycle fatigue of metals: A review. *Metals* **2021**, *11*, 204. [CrossRef]
19. Genel, K. Application of artificial neural network for predicting strain-life fatigue properties of steels on the basis of tensile tests. *Int. J. Fatigue* **2004**, *26*, 1027–1035. [CrossRef]

20. Fan, J.; Wang, Z.; Liu, C.; Shi, D.; Yang, X. A tensile properties-related fatigue strength predicted machine learning framework for alloys used in aerospace. *Eng. Fract. Mech.* **2024**, *301*, 110057. [CrossRef]
21. Feng, C.; Su, M.; Xu, L.; Zhao, L.; Han, Y. Estimation of fatigue life of welded structures incorporating importance analysis of influence factors: A data-driven approach. *Eng. Fract. Mech.* **2023**, *281*, 109103. [CrossRef]
22. Mantawy, I.M.; Ravuri, N.L.C. Predicting low-cycle fatigue-induced fracture in reinforcing bars: A CNN-based approach. *Structures* **2024**, *64*, 106509. [CrossRef]
23. Asadzadeh, M.Z.; Gänser, H.P.; Mücke, M. Symbolic regression based hybrid semiparametric modelling of processes: An example case of a bending process. *App. Eng. Sci.* **2021**, *6*, 100049. [CrossRef]
24. Selvi, S.; Vishvaksenan, A.; Rajasekar, E. Cold metal transfer (CMT) technology—An overview. *Defence Technol.* **2018**, *14*, 28–44. [CrossRef]
25. Chen, M.; Zhang, D.; Wu, C. Current waveform effects on CMT welding of mild steel. *J. Mater. Process. Technol.* **2017**, *243*, 395–404. [CrossRef]
26. *ASTM E466-96*; Standard Practice for Conduction Force Controlled Constant Amplitude Axial Fatigue Tests of Metallic Materials. ASTM: West Conshohocken, PA, USA, 2002.
27. Sharma, A.; Mohanty, U.K.; Tanaka, M.; Suga, T. Mechanism of gap bridgeability in lap-fillet laser-arc hybrid welding. *Lasers Manuf. Mater. Process.* **2021**, *8*, 355–371. [CrossRef]
28. Sun, T.; Franciosa, P.; Liu, C.; Pierro, F.; Ceglarek, D. Effect of micro solidification crack on mechanical performance of remote laser welded AA6063-T6 fillet lap joint in automotive battery tray construction. *Appl. Sci.* **2021**, *11*, 4522. [CrossRef]
29. Sugitani, D.; Mochizuki, M. Experimental study on effects of root gap and fillet size of welds on joint strength. *Q. J. Jpn. Weld. Soc.* **2013**, *31*, 104s–108s. [CrossRef]
30. Kim, D.Y.; Lee, T.H.; Kim, C.; Kang, M.; Park, J. Gas metal arc welding with undermatched filler wire for hot-press-formed steel of 2.0 GPa strength: Influence of filler wire strength and bead geometry. *Mater. Today Commun.* **2023**, *34*, 105244. [CrossRef]
31. Kim, D.Y.; Hwang, J.H.; Kim, G.G.; Kim, Y.M.; Yu, J.; Park, J. Prediction of weld tensile-shear strength using ANN based on the weld shape in Aluminum alloy GMAW. *J. Weld. Join.* **2023**, *41*, 17–27. [CrossRef]
32. OH, B. The exponential law of endurance tests. *Proc. Am. Soc. Test. Mater.* **1910**, *10*, 625–630.
33. Maddox, S.J. *Fatigue Strength of Welded Structures*, 2nd ed.; Woodhead Publishing: Abington, UK, 1991; pp. 79–81.
34. Protopopov, E.; Dobrykh, S.; Trofimova, Y.; Malenko, P.; Valter, A.; Protopopov, A. Reflection of strengthening results in values of generalized degrees of metallicity and covalence is principle to new strategy of designing alloys. *Sci. Rep.* **2020**, *10*, 2050. [CrossRef]
35. Kim, D.Y.; Kim, G.G.; Yu, J.; Kim, D.; Kim, Y.M.; Park, J. Improvement of fatigue performance by applying tandem GMAW in lap joints with gaps. *Int. J. Adv. Manuf. Technol.* **2023**, *128*, 2123–2135. [CrossRef]
36. Hwang, I.; Kim, D.Y.; Jeong, G.; Kang, M.; Kim, D.; Kim, Y.M. Effect of weld bead shape on the fatigue behavior of GMAW lap fillet joint in GA 590 MPa steel sheets. *Metals* **2017**, *7*, 399. [CrossRef]
37. Li, Y.; Yang, S.; Peng, Z.; Wang, Z.; Gao, Z. Microstructure, fatigue properties and stress concentration analysis of 6005 aluminum alloy MIG welded lap joint. *Materials* **2022**, *15*, 7729. [CrossRef] [PubMed]